Foam-induced smoothing studied through laser-driven shock waves

Dimitri Batani,[1] Wigen Nazarov,[2] Tom Hall,[3] Thorsten Löwer,[4] Michel Koenig,[5] Bernard Faral,[5]
Alessandra Benuzzi-Mounaix,[5] and Nicolas Grandjouan[5]
[1]*Dipartimento di Fisica ''G. Occhialini,'' Università degli Studi di Milano Bicocca and INFM, Via Emanueli 15, 20126 Milano, Italy*
[2]*Department of Chemistry, University of Dundee, Scotland*
[3]*University of Essex, Colchester CO4 3SQ, United Kingdom*
[4]*MPQ, Garching, Germany*
[5]*LULI, UMR No. 7605, CNRS-CEA-X-Paris VI, Ecole Polytechnique, 91128 Palaiseau, France*
(Received 12 May 2000)

The influence of foams on the uniformity of laser energy deposition has been studied by measuring laser-driven shock waves breakout from foam-aluminum layered targets. Well characterized laser nonuniformities have been produced first by using phase zone plates to get a smooth beam and then by inserting different opaque grids before the foam. Smoothing has been studied as a function of foam density and grid materials (producing different radiative effects).

PACS number(s): 52.50.Jm, 52.50.Lp, 44.30.+v, 52.35.Tc

I. INTRODUCTION

As is well known, the problem of uniformity of energy deposition in direct-drive inertial confinement fusion (ICF) is of the main importance in order to obtain ignition and high gain. In order to improve the uniformity of laser illumination, optical smoothing techniques have been introduced in last years, which include for instance the use of random phase plates [1], phase zone plates [2], kinoform phase plates [3], smoothing by spectral dispersion [4], or induced spatial incoherence [5]. Despite the considerable success of all such techniques, especially when used together, there still remains an issue of laser nonuniformity at very early times. This has been called ''laser imprint'' problem [6,7] and may have important consequences on compression uniformity at later times (and in particular on the development of Rayleigh-Taylor instability [8]) even if optical smoothing is used.

In this context, the use of low density foams has been recently proposed as a means of producing a uniform energy deposition in direct drive ICF [9]. A low density foam is inserted between the target itself (the payload material) and the laser, producing a long overcritical plasma where laser nonuniformities are homogenized by thermal smoothing. As is well known, thermal smoothing reduces the pressure variations δP, which are present at the laser deposition surface (usually the critical density layer in the plasma), by a factor

$$\Gamma = \exp(-\alpha k L),$$

where k is the wave number of the spatial perturbations of the incident laser beam, α is a factor of the order of 1 (varying according to the different models [10,11]), and L is the stand-off distance, i.e., the distance between the laser deposition layer and the ablation front. Perturbations with spatial wavelength much smaller than L are therefore completely removed by thermal smoothing.

The ''foam buffered ICF'' scheme has been firstly proposed by Dunne *et al.* [12] in preliminary experiments using a plastic foam with density $\rho = 50$ mg/cm^3 and thickness $d = 50\,\mu$m, illuminated by a laser beam at intensity $I_L \leqslant 5\times 10^{14}$ W/cm^2. According to their results, a key element for the success of the smoothing technique is the presence of a thin gold layer ($\approx$250 Å), a ''converter foil,'' before the foam layer. This layer, which rapidly evaporates and burns through, produces a high flux of soft x rays which generates a radiation-driven wave in the foam material thereby ionizing it and producing the overcritical plasma which is needed for thermal smoothing. The authors qualitatively explain their results by saying that, in the case where the foam is present, the stand off distance L must be replaced by the all thickness of the foam layer, which has been transformed in an overcritical plasma layer, so that the factor Γ is strongly decreased.

Even if such explanation is plausible, still many points need to be studied in this context, in particular the influence of foam parameters (density, thickness, etc.) and that of x-ray radiation on the effectiveness of smoothing. Also it is very important that the radiation field is able to produce the desired overcritical plasma without, at the same time, inducing a preheating of the payload material after the foam. Indeed in ICF it is fundamental to minimize the drive energy in order to compress the target along a low isentrope and reach a high gain. Thus the preheating of the thermonuclear fuel must be avoided, especially in the early stages of the implosion.

Another point is that in Ref. [12] no attempt was made to control the laser beam nonuniformities and only the nonuniformities naturally produced by the hot spots present in the laser beam profile and by the smoothing technique were used. This, although not necessarily too important in this stage of the experiments, could be indeed very interesting in verifying what the scale is of the nonuniformities that are really smoothed with the foam technique.

With this aim we realized the experiment presented in this paper. Its schematic setup is shown in Fig. 1 with the following basic elements.

(i) The use of foams of density from 30 to 200 mg/cm^3 to study the smoothing effects as a function of foam density (instead the foam thickness was fixed and $\approx$60 μm).

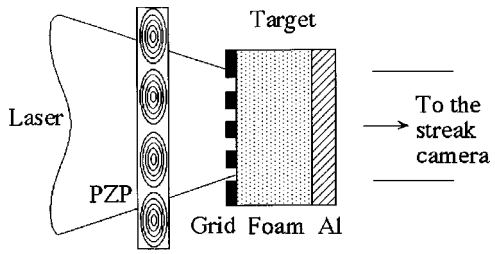

FIG. 1. Scheme of the experimental setup at LULI.

(ii) The use of well-known nonuniformities which have been produced first by using phase zone plates to produce a smooth and flat beam profile [2], and then by inserting opaque grids (9 μm thick) before the foam. In this first experiment only grids with a 60 μm spacing have been used.

(iii) The use of grids of different materials in order to change the radiation emission (concerning both the intensity and the spectral distribution of x rays). Then in our experiment the grid had the double goal of producing the laser nonuniformities which we wish to smooth away and the radiation which should create the overcritical plasma.

The use of 9 μm thick steps was required to avoid the complete ablation of the grid material during the laser pulse, in order to maintain the nonuniformity of irradiation during all the interaction. On the other hand this implies a regime in which smoothing due to radiation-driven ionization of the foam, refraction effects on laser beams in the nonuniform plasma corona, nonlinear interactions of shocks, and nonlinear effects in x-ray illumination from the grid sides, all play a role. We think, however, that the interpretation of the experimental data presented in Sec. III mainly relies on smoothing, due to the different time scales implied in the different phenomena, as will be shown in Sec. IV A.

In the experiment a streak camera was used as diagnostic to detect the shock breakout from the layered targets made of foam on the laser side and an aluminum layer on the rear side (Fig. 1). Although aluminum is not a material used in ICF foam-buffered targets, it allows us to simulate the realistic situation of shock transmission from the low density foam to a denser payload material. The great advantage of aluminum is that its equation of state (EOS) is well known [13], which makes it a typical reference material in shock experiments.

Such an experimental scheme allows smoothing effects to be measured as already shown by Kado and Tanaka [14] in an experiment on thermal smoothing without foams. Indeed if there were a perfect smoothing of laser nonuniformities, then a flat shock breakout would be detected on the target rear side. On the contrary, if the smoothing is not perfect, an early shock breakout must be detected where the shock is stronger and a delayed shock breakout in correspondence of the other points. In the case of Ref. [14], the smoothing effect was related to the experimentally measured difference in shock velocity. More precisely the smoothing factor Γ is calculated using the dependence $P \approx I^{2/3}$ and $P \approx D^2$ (according to Refs. [15] and [16]), as

$$\Gamma = \frac{\delta D}{\overline{D}} \frac{I_{\max}^{2/3} + I_{\min}^{2/3}}{I_{\max}^{2/3} - I_{\min}^{2/3}},$$

where $\overline{D}$ is the average shock velocity, $I_{\max}$ and $I_{\min}$ are the maximum and minimum values of the laser intensity on target, and

$$\delta D = D_{\max} - D_{\min}.$$

We note that in our case, unlike in Ref. [14], we have $I_{\min} = 0$, and then Γ is simply given by $\delta D/\overline{D}$.

II. EXPERIMENTAL SETUP

The experiment was performed using three beams of the Laboratoire pour l'Utilisation des Lasers Intenses (LULI) Nd laser (converted at $\lambda = 0.53\,\mu$m, with a total maximum energy $E_{2\omega} \approx 100$ J). The pulse was Gaussian in time with a full width half maximum (FWHM) of 600 ps. All beams had a 90 mm diameter and were focused with a $f = 500$ mm lens onto the same focal spot. We used phase zone plates (PZP) in order to eliminate large scale spatial intensity modulations and produce a flat-top intensity profile [2]. Since the smoothing effect introduced by the foam varies with its density, the use of PZPs was necessary in our experiment in order to get the same irradiation conditions for any foam density. Our optical systems (PZP+focusing lens) produced a focal spot of 400 μm FWHM, with an $\approx$200 μm wide flat region in the center, corresponding to a laser intensity $I \approx 3-5 \times 10^{13}$ W/cm^2. Such large focal spots were needed to reduce two-dimensional (2D) effects because the total thickness of the target was of the order of 80 μm.

The target was made with an Al layer (13.2 μm thick) over which a foam layer was realized with a technique developed at Dundee University [17]. The monomer used in our experiments was TMPTA (trimethylol propane triacrylate, $C_{15}H_{20}O_6$). Foams of thickness 54 to 66 μm and densities from 30 to 200 mg/cm^3 were produced, all corresponding to overcritical plasmas in case of full ionization. Finally, grids with spacing 30 μm and step 30 μm were used (except for the plastic grids which had, respectively, 27.5 and 32.5 μm). Their thickness was 9 μm and they were realized in different materials, i.e., gold, copper, and plastic (this last to produce a small x-ray flux and low radiative effects in the foam).

Notice that the grid transparency is $\approx \frac{1}{2}$ so that the average laser intensity is $\overline{I} = (I_{\max} + I_{\min})/2 = I_{\max}/2 \approx 2 \times 10^{13}$ W/cm^2. The average value of $\overline{I}$ will then correspond to an average pressure $\approx$4 Mbar corresponding to what can be obtained from scaling laws [15] for our laser and target parameters:

$$P \approx 8.6 (I/10^{14})^{2/3} \lambda^{-2/3} (A/2Z)^{13},$$

where P is in Mbar, λ in μm, and I in W/cm^2.

III. EXPERIMENTAL RESULTS

Figure 2 shows different streak camera images obtained with foams of density 30, 100, and 200 mg/cm^3 and copper grids. We can see a time fiducial on the top left of each image. Instead Fig. 3 shows three results obtained for $\rho = 50$ mg/cm^3 and different grid materials. Such images, and the others obtained in the experiment, show how the smoothing effect is affected both by the grid material and the foam

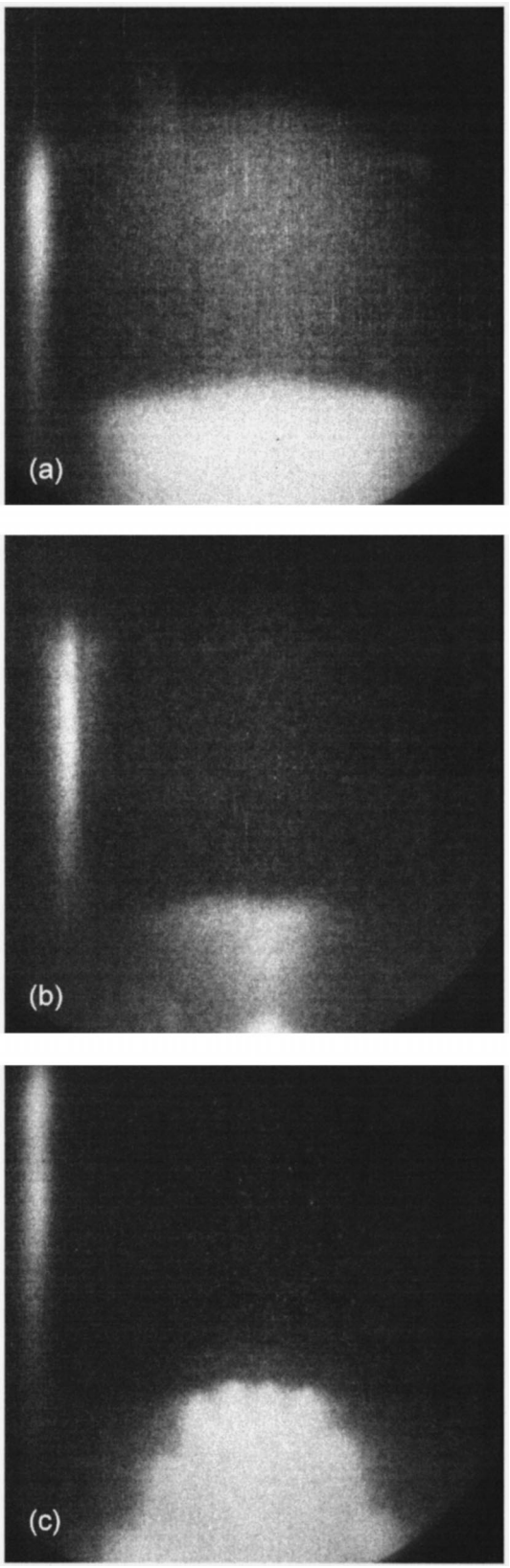

FIG. 2. Streak camera images obtained with grid+foam+Al targets (grid spacing≈60 μm, foam thickness≈60 μm, Al base 13.2 μm) in the case of a Cu grid and foams of density (a) 30, (b) 100, and (c) 200 mg/cm^3. The laser energy was, respectively, 92, 83, and 94 J. A time fiducial can be seen on the top left of each image. Time flows up to down and the dimensions of the figure are 1.8 ns and 800 μm (in this and in all following streak camera pictures).

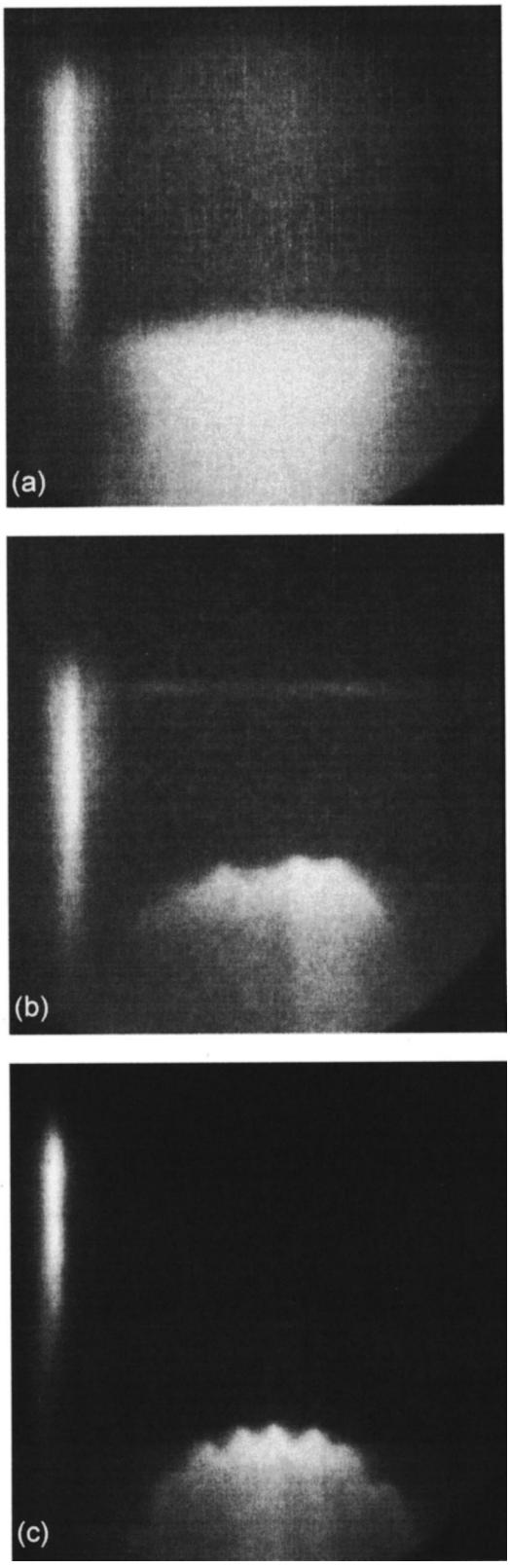

FIG. 3. Streak camera images obtained with grid+foam+Al base targets (grid spacing≈60 μm, foam thickness≈60 μm, base 13.2 μm) in the case of a $\rho=50$ mg/cm^3 foam and grids of different materials: (a) Cu, (b) Au, and (c) CH. The laser energy was, respectively, 94, 90, and 79 J. A time fiducial can be seen on the top left of each image.

density. Also, the results in Figs. 2 and 3 clearly show that in some cases, the presence of the foam layer allows a smoothing of laser-imprints nonuniformities of the order of 100%, i.e., the shock breakout signal appears to be practically flat. This is true even with the very large scale nonuniformities used in our experiment ($\approx$60 μm from peak to peak) and will be obviously easier in the case of smaller nonuniformities, which are more easily smoothed by thermal transport.

However, at the same time two features seem surprising: first the smoothing effect seems better in copper as compared to gold, while gold is known to have a higher laser-to-x-rays conversion efficiency; and second, a foam density of 30–50 mg/cm^3 seems to produce a better smoothing than a 100–200 mg/cm^3 foam, although a denser plasma will be certainly formed in this last case.

We can also see from Fig. 3 that a bigger preheating is present in the case of a copper grid, and that this preheating is more important at low foam density, as can be seen by comparing Figs. 2(a) and 3(a).

Before explaining our results, we want to point out that the interpretation of such images is not obvious due to the absence of a ''blank'' reference. Indeed, even if small, radiation effects cannot be completely excluded in the case of plastic grids. Moreover, in our scheme thermal smoothing is not only active in the foam itself but also in the payload material (we will see how this has a strong influence on experimental results). Finally, the smoothing effect, which is evident in the images in Figs. 2 and 3, is not only due to thermal smoothing since a geometrical effect is also present, which tends to smooth the shape of the shock wave as it propagates through the material. This purely 2D geometrical effect tends to produce a flat shock front due to the superimposition of secondary shock waves, in analogy with what happens with light waves according to the Huygens principle.

In order to test the importance of such effects we realized the shots shown in Figs. 4(a) to 4(c). The first two pictures show streak camera shock breakout images obtained with targets without foam, in which the grid was directly glued on the Al layer. This eliminates both the thermal smoothing and the geometrical smoothing effect in the foam (but not, of course, smoothing in Al). We see in all cases the laser imprinting on the cold target, irrespective of the grid material. We also note, as in the case of targets with foam, the bigger preheating in the case of copper grid. The third one [Fig. 4(c)] shows instead a shock breakout obtained with a target without foam in which the grid was kept at a distance of 50 μm from the Al layer. In this way thermal smoothing in the foam is avoided while 2D smoothing effects still play a role (anyway 2D geometrical smoothing now acts on the laser illumination itself through vacuum and not on shock waves through the foam).

Even if the shots shown in Fig. 4 do not constitute a blank case for the images of Figs. 2 and 3, they give at least a sort of qualitative evidence that smoothing effects are stronger when the foam is present. Also, the dependence on foam density and material in Figs. 2 and 3 shows that such smoothing effects are not only due to geometrical effects.

Figure 5 summarizes the results of Figs. 2–4. Here the maximum difference δt in shock arrival along the shock front is shown for the different cases. Such temporal differ-

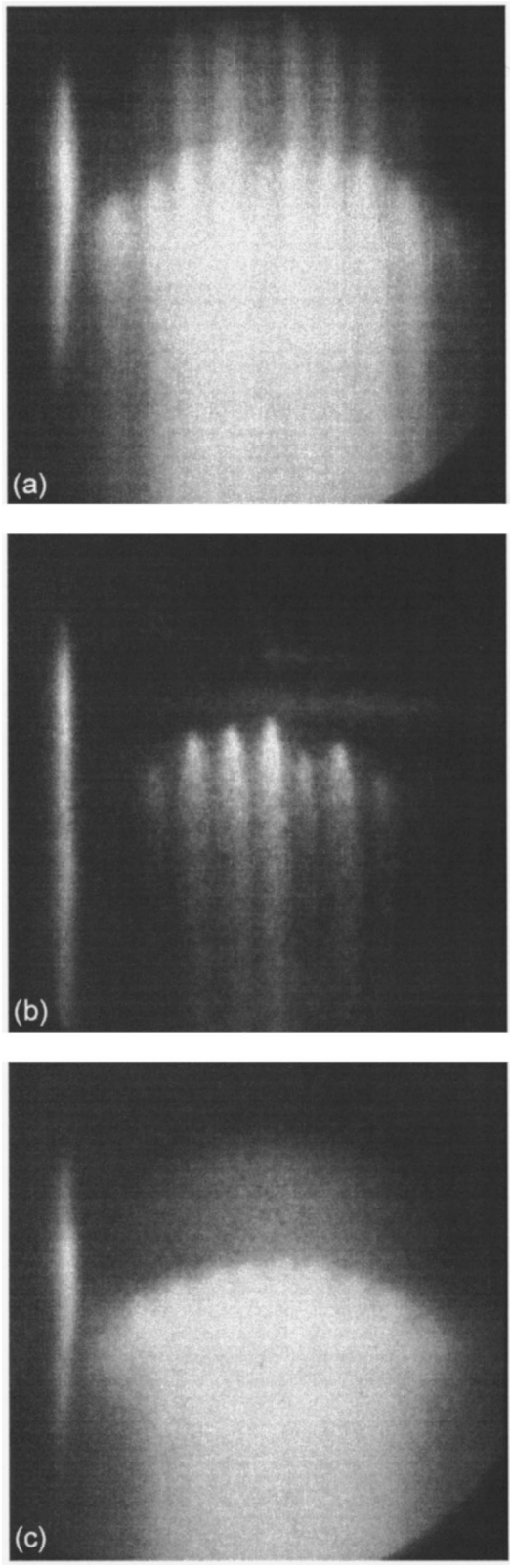

FIG. 4. Streak camera images obtained with aluminum targets (thickness 13.2 μm) without foam in which a Cu grid (a) and an Au grid (b) was directly glued on the Al layer. The third image (c) shows a shock breakout obtained with a target without foam in which the grid was kept at a distance of $\approx$ 50 μm from the Al layer. The laser energy was, respectively, 55, 54, and 52 J.

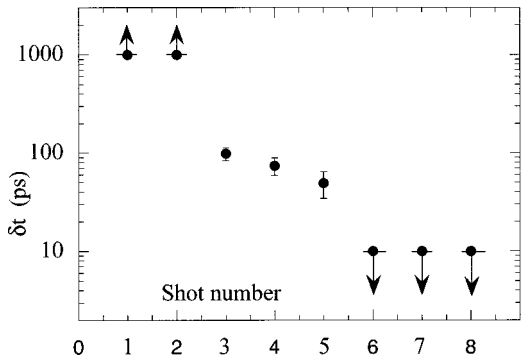

FIG. 5. Differences δt in shock arrival time across the central region of the shock front for different cases: (1) no foam, Cu grid; (2) no foam, Au grid; (3) 50 mg/cm^3 foam, CH grid; (4) 50 mg/cm^3 foam, Au grid; (5) 200 mg/cm^3 foam, Cu grid; (6) 50 mg/cm^3 foam, Cu grid; (7) 100 mg/cm^3 foam, Cu grid; (8) 30 mg/cm^3 foam, Cu grid.

ence δt is connected to the difference in shock velocity δD and hence to the smoothing parameter Γ. The cases of Figs. 2(a), 2(b), and 3(a) correspond to $\delta t \leqslant 10$ ps, i.e., no difference in shock arrival time is detected within the temporal resolution of the recording apparatus (10 ps as determined by streak camera sweep speed and slit size). On the contrary, in the case of Figs. 4(a) and 4(b) no homogenization of shock breakout was evidenced, i.e., no breakout signal was detected in the position corresponding to the grid steps and hence $\delta t \geqslant 1$ ns (as connected to the temporal window in the recorded streak camera image). Intermediate differences δt correspond to Figs. 2(c), 3(b), and 3(c).

Finally Figs. 6 and 7 show the influence of laser intensity, respectively, in the case of targets with a gold grid directly placed on the Al layer and in the case of plastic grid–50 mg/cm^3 foam targets. In both cases a better smoothing is observed for higher intensity.

IV. DISCUSSION

In order to explain our experimental data, we tried to develop a simple analytical model. As seen in Sec. I, the actual experimental situation is quite complicated. We are interested in the radiation-driven smoothing of the nonuniformities created with the grid, but at the same time other phenomena play a role, such as refraction effects on laser beams and nonlinear interaction of shocks. The complete numerical simulation of all these phenomena is beyond the scope of the present paper. Moreover, it is very difficult to imagine how these phenomena can bring some uniformization to the shock breakout. On the contrary, they would very likely produce stronger nonuniformity. For instance in the case of refraction, the nonuniform plasma density will probably constitute the seed for beam filamentation which will produce a laser illumination which is even less uniform than the initial one. This suggests that the physical interpretation of our experimental data is probably based on a somewhat ''simpler'' physical mechanism.

Therefore in order to study the problem, we firstly developed a simple semianalytical ''heuristic'' model to estimate x-ray emission from the grid, x-ray absorption in foam and Al layers, and the density and temperature profiles in the

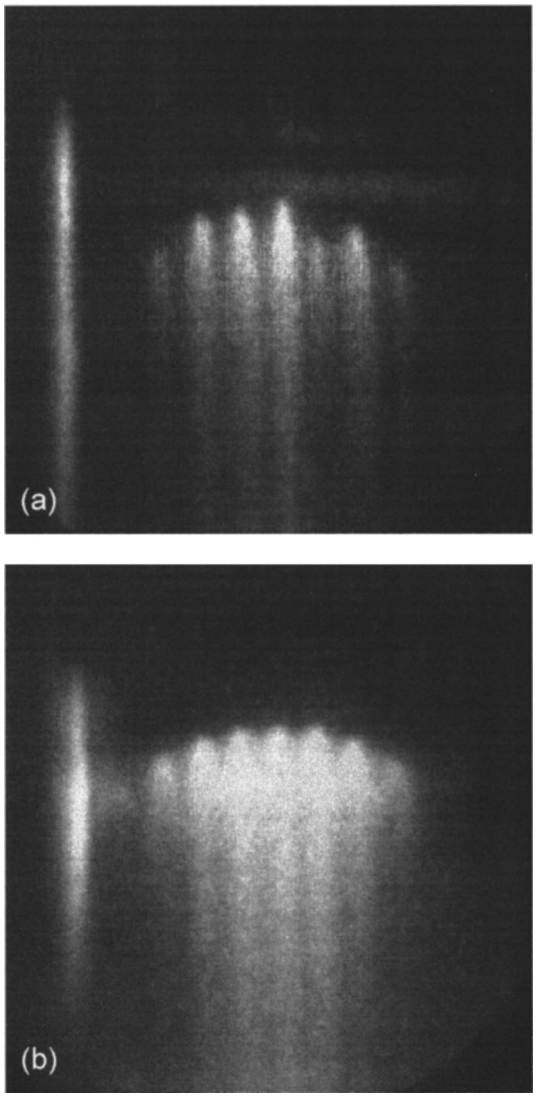

FIG. 6. Streak camera images obtained with aluminum targets (thickness 13.2 μm) without foam, in which a Au grid was directly glued on the Al layer. The laser energy was (a) 54 J ($I = 4.2\times10^{13}$ W/cm^2) and (b) 85 J (6.5×10^{13} W/cm^2). A better smoothing is observed for higher intensity.

target. We also used the computer code MULTI (multigroup radiation transport in multilayer foils) [18] to run hydrodynamic-radiative simulations which have been compared to the results of the semianalytical model. Although both MULTI and the model assume local thermodynamical equilibrium (LTE) conditions, in reality much of the plasma will be far from LTE (as shown for instance in Ref. [19]). In this respect both our semianalytical model and MULTI simulations represent a much simplified description of the physical reality and are simply used on a heuristic basis.

The results obtained with the two models agree quite well with each other, which gives a good reason to trust our interpretation. We think in particular that the use of MULTI alone would be questionable due to the very low precision with which opacities are known. This uncertainty plays a double role since first the emission from the grid material must be estimated and then its absorption in the foam. In order to overcome such uncertainties we used published data [20–26] for the emission spectra of C, Cu, and Au and the

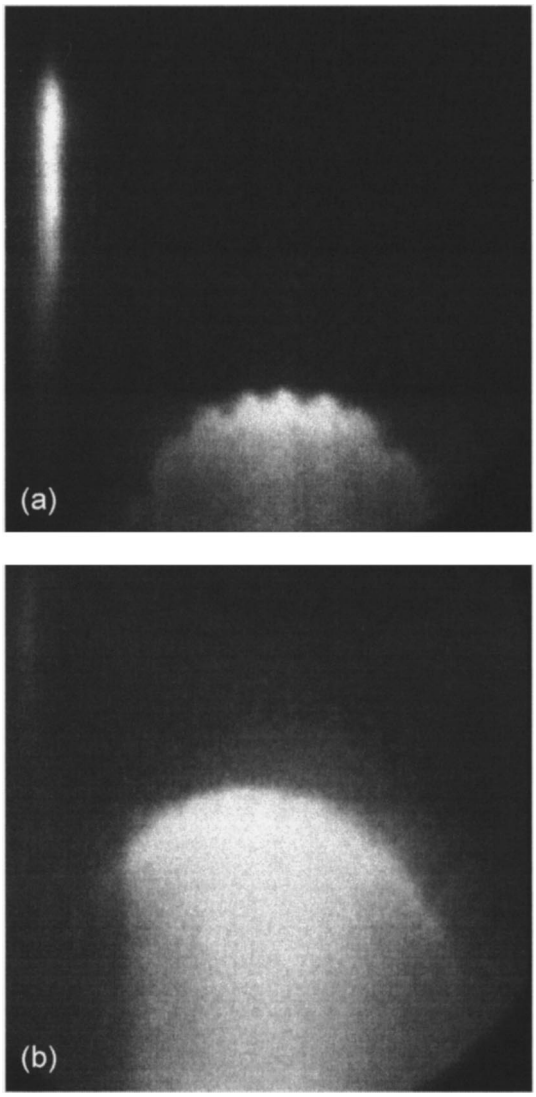

FIG. 7. Streak camera images obtained with grid+foam+Al base targets (grid spacing≈60 μm, foam thickness≈60 μm, base 13.2 μm) in the case of a CH grid and 50 mg/cc foam layer. The laser energy was (a) 79 J ($I=6.1\times10^{13}$ W/cm^2) and (b) 98 J ($I=7.5\times10^{13}$ W/cm^2). A better smoothing is observed for higher intensity.

laser to x-rays conversion efficiency. Then, neglecting for the moment foam hydrodynamics, we propagated the x-ray flux through the foam. The assumption of neglecting hydromotions is justified as long as the phenomena induced by x rays absorption take place over a much shorter time scale, a condition which we will verify in the next section and which is anyway the idea at the basis of foam-buffered ICF.

A. Semianalytical model

Experimental data on Cu and Au conversion efficiency η reported in literature [20–26] show that Au conversion efficiency is bigger than Cu (a higher x-ray flux is produced): $\eta\approx50\%$ in the case of gold against 30% for copper. However, when x-ray spectra are analyzed, the spectrum of copper extends to higher energies, having non-negligible emission up to ≈4.5 keV as compared to ≈3 keV for gold. Also, in an intensity range comparable to the one used in our experiment, Au emission is centered around 0.7 keV while Cu is characterized by strong emission between 1 and 1.5 keV.

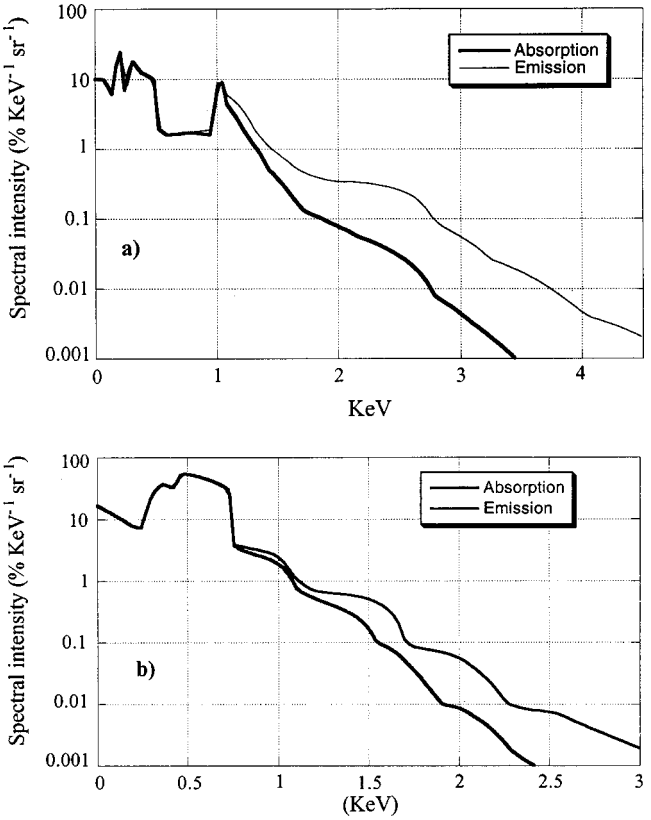

FIG. 8. Convolution of the experimental emission spectra (from Ref. [21]) with the foam absorption for a layer of 60 μm and 100 mg/cm^3, (a) Cu grid; (b) Au grid.

The conditions under which these experimental spectra have been obtained are not far from those of our experiment. Moreover, they refer to emission on the laser side, which is really what is interesting in our case. Indeed due to the large thickness of the grid, no x rays will be emitted on the back side of the grid steps.

In order to discuss the relevance of this simplified model of x-ray emission for the interpretation of our results, one should consider that while the fine details of x-ray emission depend on the irradiation and geometrical parameters in a complicated way, the gross features are not so sensible, in particular (for laser intensities not too far from those used in our experiment), they mainly depend on the irradiated material. We refer to the presence of characteristic *K*, *L*, *M*, ⋯ peaks in x-ray emission which is what is really important for efficiently coupling the x-ray radiation to the foam and Al layers. Within these limits, MULTI simulations also reproduce the main features of the experimental spectra found in the literature.

Figure 8 shows the convolution of the experimental emission spectra [22] with the foam absorption for a layer of 60 μm and 100 mg/cm^3 [(a) copper grid; (b) gold grid]. The analysis of such graphs for different foam densities, and the comparison with the emission spectra (also shown in the same figure), shows that x rays can be approximately divided in two groups: low-energy x rays ($h\nu<1$ keV) which are completely absorbed in the foam contributing to its ioniza-

tion and heating, and higher-energy x rays ($h\nu \geqslant 1$ keV) which do not contribute much to these phenomena being less attenuated, but may be transmitted to the payload material after the foam. Integrating the graphs in Fig. 8 over photon energies it is possible to calculate that ≈31% and ≈48% of the laser energy is absorbed in the 60 μm–100 mg/cm^3 foam layer in the case of Cu and Au, respectively (these figures change to ≈28 and 45% in the case of 50 mg/cm^3 foam). Such energy, if uniformly distributed over the whole foam thickness, would be sufficient to produce an overcritical plasma due to heating and ionization of the foam. However, this is not what happens in reality since x rays are produced over a certain duration and, above all, because most of absorbed x rays are really absorbed in the very first foam layers due to their very low penetration.

More precisely, assuming a temporally flat x-ray pulse of duration equal to the laser pulse t_L, we find that the energy deposited in a foam layer between x and $x+dx$ in the time dt due to the photons of energy $h\nu$, is given by

$$dE(x,t,h\nu) = g\pi(E_L/t_L)\left[\int_0^{\pi/2} d\vartheta(\cos\vartheta)^{\alpha}\sin\vartheta\right] \times I(h\nu)\mu\rho e^{-\mu\rho x} dt\, d(h\nu) dx,$$

where g is a factor that takes into account the geometry of the target (a grid in our case), E_L is the laser energy (which must be divided by 2 to take into account the grid transparency), the factor $(\cos\vartheta)^{\alpha}$ describes the angular distribution of emitted x rays (notice that *a priori* α may be different for different photon energies), and μ and ρ are, respectively, the foam absorption coefficient and density.

Here the transparency of the foam is calculated by using the absorption coefficients μ for cold foam, reported in the official web site of the Center for X-Ray Optics (http://www-cxro.lbl.gov/) of the Lawrence Berkeley National Laboratory (LBNL) and obtained using Henke's model [27]. Again, this assumption is justified only as long as a fast x-ray-induced ionization is observed.

Assuming for sake of simplicity $\alpha = 1$ for all photon energies and $g = 1/2$, we finally get a formula which allows us to calculate energy deposition as a function of time, space, and frequency. From the energy $dE(x)$ deposited in a foam layer of thickness dx, we can then calculate the ionization degree Z^* (i.e., the electron density n_e) and the plasma temperature T consistently by using More's formula [28] for Z^* (which is derived from the Thomas-Fermi model) and equipartion of energy to calculate T sharing the energy between all the particles. We neglect the energy spent in ionization and get

$$dE(x) = \tfrac{3}{2}(1+Z^*)n_i T\, dV.$$

Here $n_i = n_e/Z^*$ is the ion density which, due to the approximation of neglecting hydromotion, is only related to the initial foam density. The calculations are reiterated until consistent values of Z^* and T are found. This calculation has been used to obtain the results in Figs. 9 and 10 which show, respectively, the temperature and density profiles for Cu and Au grids and foams of different initial density (for the sake of brevity we only report the cases of 50 and 100 mg/cm^3 foams).

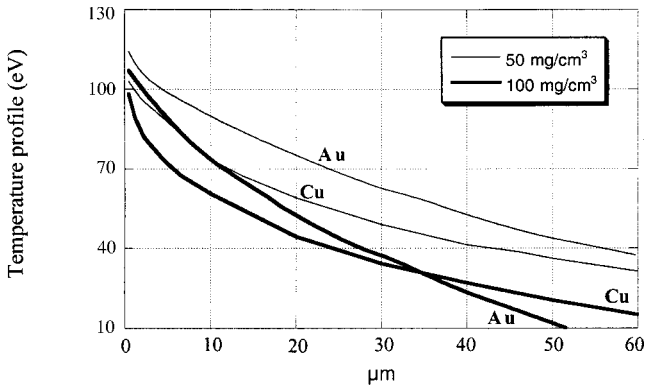

FIG. 9. Temperature profiles in the case of Cu and Au grids and foams of initial density 50 and 100 mg/cm^3.

Some very interesting conclusions can be drawn from the analysis of such figures. First the temperatures reached in the foam layer are bigger in the 30–50 mg/cm^3 case than in the 100–200 mg/cm^3 case. Indeed the x-ray energy absorbed in the 30–50 mg/cm^3 case is slightly less but it is shared between a smaller number of particles. On the other side the plasma is well overcritical in both cases (in our experiment $n_c \approx 4\times 10^{21}$ cm^{-3}). We think that the better smoothing effect observed in the 30–50 mg/cm^3 case is related to the bigger temperature which causes a drastic increase in the electron mean free path and related quantities such as thermal conductivity. This is true for both Cu and Au grids.

We also see that in the case of 100–200 mg/cm^3, at a certain distance, the density and temperature of the foam plasma become bigger with Cu than with Au. This effect is due to the fact that most soft x rays are absorbed before this layer and after it the contribution from harder x rays becomes dominant (of course it is not observed in the 30–50 mg/cm^3 case due to the lower overall absorption). After the foam, such x rays are likely to be transmitted to Al and cause a preheating of this layer. In order to verify this hypothesis we applied the model to Al obtaining the results shown, in the case of a 100 mg/cm^3 density foam in Fig. 11. We see that indeed there is a non-negligible preheating of Al in the case where a Cu grid is used. The discontinuity in plasma temperature at the foam-Al interface is due to the discontinuity in the absorption coefficient: the harder x rays, which propagate almost freely in the foam, are abruptly stopped in Al. In

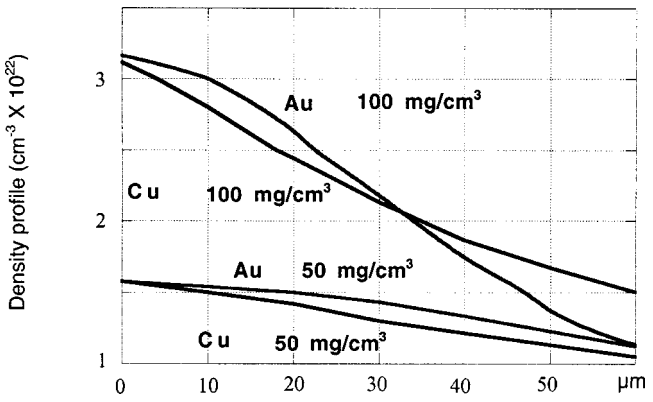

FIG. 10. Density profiles in the case of Cu and Au grids and foams of initial density 50 and 100 mg/cm^3.

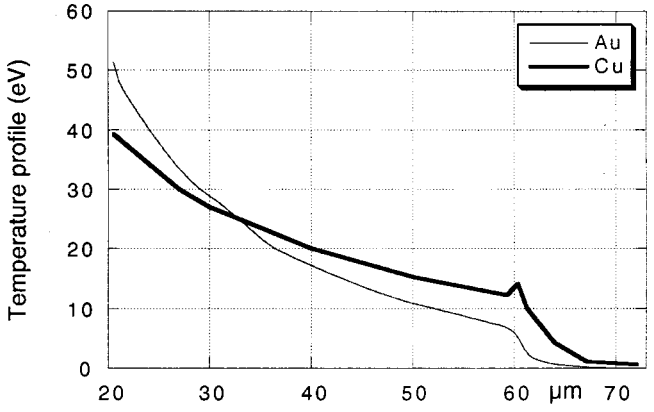

FIG. 11. Temperature profiles in the foam layer ($\rho = 100$ mg/cm^3) and in the aluminum base in the case of Cu and Au grids. The foam-Al interface is at 60 μm.

the case of a 50 mg/cm^3 foam, the model does not show such discontinuity, but higher temperatures are reached because a larger x-ray flux is reaching the Al layer.

Finally Fig. 12 shows the time evolution of the electron density profile. The velocity of this ''ionization wave'' can be estimated by noting that the critical point moves a distance equal to ≈ 50 μm in 50 ps from which we get a velocity >1 μm/ps. Such velocity is much bigger than the velocity of any hydrodynamic wave. For instance, the shock wave velocity in the foam, in our conditions, is at most of the order of ≈ 100 μm/ns (as can be extrapolated from Ref. [29]). Also it is much bigger than the ablation velocity, i.e., the velocity at which matter is transformed into a hot plasma by laser heating. At early times this must be calculated using the model for absorption at the critical surface [15]; at later times, when a long plasma corona has developed, absorption becomes nonlocalized and the ablation rate of the foam is given by [30]

$$\dot{m} = 4.5 \times 10^{-6} I^{3/4} \lambda^{-1/2} t^{-1/4},$$

where now t is in ns and $\dot{m}$ is in g cm^{-2} s^{-1}. In both cases we get an ablation velocity $v_a(t) = \dot{m}/\rho$ of the order of 40 μm/ns for a 50 mg/cm^3 density. These two observations seem to justify *a posteriori* the assumption of neglecting the hydromotion of the foam.

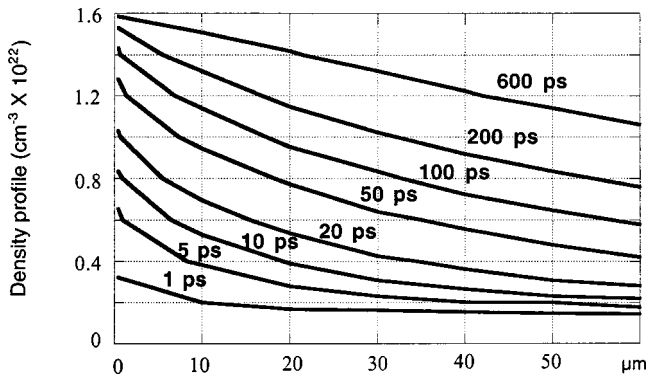

FIG. 12. Time evolution of the electron density profile in the case of a 50 mg/cm^3 foam-Cu grid target. The ''ionization wave'' has a velocity of about 2 μm/ps.

B. MULTI simulations

Simulations were performed with the one-dimensional hydrocode MULTI [18] which takes radiation transfer into account by using a multigroup radiative diffusion model. We have used the SNOP opacity tables (steady-state non-LTE opacities) [31] for Cu and Au, and the Los Alamos opacity data base (TOPS opacity tables [32]) for TMPTA. Also, for TMPTA, we have used the SESAME EOS tables [13] for plastic where the initial density has been set to the experimentally measured foam density. An additional difficulty is that using a monodimensional (1D) code is not possible to simulate the real situation in which a grid is put before the foam layer. Then, to simulate our situation in which the target is subject at the same time to laser and x radiation, we calculated separately (always with MULTI) the emission spectrum of a Cu or Au target and then we included the calculated X radiation in the simulation, contemporary to laser radiation. Neglecting 2D aspects of the problem, we only wanted to analyze the effect of the radiation flux on the foam and the formation of an overcritical plasma characterized by some density and temperature scale lengths.

We underline again that emission spectra calculated with MULTI agree quite well with the experimental spectra, the code reproducing the main features of emission such as characteristic peaks and conversion efficiency. The fine details of emission are not reconstructed by the multigroup average-atom approach used in MULTI, but this is not really important since the interaction does not seem to depend on such fine details.

Figure 13 shows the time behavior of target rear side emissivity calculated with MULTI and compared with the experimentally observed results, i.e., with the time behavior of emissivity recorded with the streak camera (a vertical cut of the streak camera images in one fixed position). Both the simulations and the experimental results show an increase in emissivity before shock breakout; in both cases this emission is visible ≈ 1 ns before shock breakout and is a clear signature of target preheating as shown in various recent works [33,34].

Even if simulations neglect the 2D aspects, nevertheless they give us important information, such as the temperature profile in the plasma and the hydrodynamic time scales. From Fig. 13 we can see that time scales reproduced by simulations do not agree with the observed time scales, even if the qualitative behavior of the signal is quite similar to experimental data. The code gives a shock breakout at 400 ps after laser peak, while experimental data indicate a bigger delay, of about 1 ns. This is due to the fact that the code does not take lateral energy transport into account and that the presence of a grid in the real case gives, as previously seen, an average laser intensity of about 2×10^{13} W/cm^2, while in these 1D simulations a laser intensity 5×10^{13} W/cm^2 was used.

Anyway MULTI simulations confirms quite well the results obtained with the semianalytical model: no formation of a radiative wave was evidenced in the simulations, but plasma temperature was characterized by a semiexponential profile. Also, plasma temperature decreases with the distance and abruptly increases at the foam-Al interface. This seems to support our interpretation of the role played by radiation and foams in the smoothing of laser energy deposition.

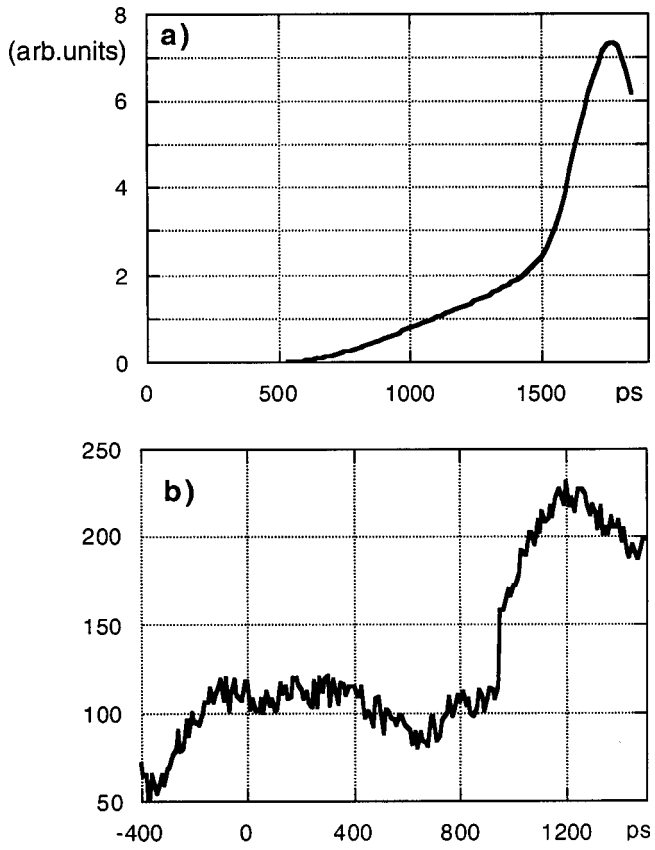

FIG. 13. (a) Time behavior of target rear side emissivity calculated with MULTI for a 50 mg/cm^3 foam-Cu grid target irradiated with a laser intensity $I=5\times10^{13}$ W/cm^2. The laser peak is at 1200 ps. (b) Time behavior of emissivity recorded with the streak camera, a vertical cut of the image in Fig. 3(a). The laser peak is at 0 ps.

V. CONCLUSIONS

In conclusion, we presented results concerning foam-induced smoothing of laser energy deposition. We can see the following.

(i) How a very fast ionization of the foam material is predicted, mainly as a consequence of the low density of foams. This is in agreement with what is observed in Refs. [35] and [36]. In all cases of interest the initial foam mass density and the degree of ionization effectively reached seems to be enough to quickly produce an overcritical plasma. The very rapid formation of an overcritical plasma is essential in order to get an effective thermal smoothing. However, no real radiative wave is observed in the simulations, at all times plasma density maintaining a quasiexponential profile, i.e., closely following the absorption of x rays from the plasma corona.

(ii) How the observed better smoothing, which is obtained with Cu as compared to Au is probably an indirect effect of the stronger preheating induced in Al in the case of Cu as observed in the experimental results of Fig. 3. Target preheating obtained with Cu produces a change in Al, thereby strongly increasing the thermal smoothing effectiveness in the Al heated layer. It must be recalled indeed that the thermal smoothing effect observed at the target rear side through shock wave detection does correspond to the whole foam plus Al layers. However, the situation with Cu is worse with respect to its applicability to the idea of foam-buffered ICF. Indeed, it is true that target preheating must be avoided in ICF since it will move the target material off the isentrope with a significant loss of compression efficiency. The effective thermal smoothing in the foam layer alone is probably about the same with Cu and Au since in both cases plasmas of similar density and temperature are produced (with a slight preference towards the use of Au).

(iii) How not only the foam density plays a role in the smoothing effect, i.e., the fact that the plasma formed is over critical. Also its temperature is very critical. A higher temperature will increase the electron mean free path and lateral energy transport, thereby contributing to a more effective thermal smoothing. This can easily be seen by looking at the formula for thermal conduction

$$K\propto\frac{T^{5/2}}{Z^*\ln\Lambda}$$

(where $\ln\Lambda$ is the Coulomb logarithm) and justifies the fact that smoothing is more effective at 30–50 mg/cm^3 than at 100–200 mg/cm^3. In this last case indeed the temperatures reached in the plasma are a factor of 2–4 lower than with 30–50 mg/cm^3.

This conclusion is in agreement with those of Ref. [37], which show how smoothing derives principally from the high thermal conductivity of the heated foam. However, a complementary explanation of our data is also possible, based on the work by Velikovich *et al.* [38] (but see also Refs. [39,40]) and probably the mechanism explained in this paper acts at the same time with the increased thermal conductivity due to the higher temperature in the lower density foam.

The authors have studied analytically and numerically the growth of mass perturbations during the shock transit time. Their model predicts that in the presence of thermal smoothing the mass variation δm saturates at a certain time, instead of growing indefinitely. There thermal smoothing within the conduction zone is represented with an exponential function:

$$\delta p_a/p_a=\varepsilon\exp(-t/t_1),$$

where δp_a is the perturbation of ablation pressure, ε is the characteristic dimensionless amplitude of imprint, and t_1 is the ''thermal smoothing time,'' typically of the order of 1 ns. In the strong-shock limit the saturation value $\delta m_{\rm sat}$ is found to scale as $t_1\rho_0^{1/2}$, where ρ_0 is the initial density of the target. The scaling with density is of particular interest because it is related to the opportunity of decreasing the imprint saturation level.

Coming back to the explanation of our data, we have seen how lowering the foam density implies a higher temperature in the plasma (and a more effective thermal smoothing). In the model of Velikovich *et al.* [38] the influence of ρ_0 on the plasma temperature is resumed in the parameter t_1. A more effective thermal smoothing implies a lower value for t_1 and consequently a smaller $\delta m_{\rm sat}$. Hence in the case of radiation-driven smoothing, the target density plays a double role in determining $\delta m_{\rm sat}$, even if keeping a fixed value of ρ_0 and changing the grid material possibly allows us to study the two effects separately.

In conclusion, our results point out the importance of carefully choosing the foam and the converter foil parameters (in particular, foam density and grid material). Of course, it is not immediate to extrapolate our case, in which the grid acts both for the introduction of nonuniformities and the generation of x rays, to the case where a real converter foil is used. All the qualitative aspects connected to the shape of the x-ray spectrum, observed in our experiment, of course remain valid in the other case. At the same time, our results clearly show that thermal transport in the overcritical plasma produced from a low density foam coupled to x-ray irradiation (radiation driven) allows a smoothing of laser-imprints nonuniformities of the order of 100%. This is true even with the very large scale of nonuniformities used in our experiment ($\approx$60 μm from peak to peak) and will be obviously easier in the case of smaller nonuniformities, which are more easily smoothed by thermal transport.

ACKNOWLEDGMENTS

The experiments presented here have been realized at LULI and supported by the E.U. ''Access to Large Scale Facilities'' program under Contracts No. CHRX-CT93-0377, No. CHRX-CT93-0338, and No. ERB-CH-CT92-0006.

[1] Y. Kato, K. Mima, N. Miyanaga, S. Arinaga, Y. Kitagawa, M. Nakatsuka, and C. Yamanaka, Phys. Rev. Lett. **53**, 1057 (1984).
[2] M. Koenig, B. Faral, J. M. Boudenne, D. Batani, S. Bossi, and A. Benuzzi, Phys. Rev. E **50**, R3314 (1994).
[3] S. N. Dixit, I. M. Thomas, M. R. Rushford, R. Merrill, M. D. Perry, H. T. Powell, and K. A. Nugent, ICF Quart. Rep. **4**, 152 (1994).
[4] S. Sckupsky, R. W. Short, T. Kessler, R. S. Craxton, S. Letzring, and J. M. Soures, J. Appl. Phys. **66**, 3456 (1989).
[5] R. H. Lehmberg and S. P. Obenschain, Opt. Commun. **46**, 27 (1983).
[6] M. H. Emery, J. H. Gardner, R. H. Lehmberg, and S. P. Obenschain, Phys. Fluids B **3**, 2640 (1991).
[7] M. Desselberger, T. Afshar-rad, F. Khattak, S. Viana, and O. Willi, Phys. Rev. Lett. **68**, 1539 (1992).
[8] R. J. Taylor, J. P. Dahlburg, A. Iwase, D. E. Fyfe, J. H. Gardner, and O. Willi, Phys. Rev. Lett. **76**, 1643 (1996).
[9] M. Desselberger, M. W. Jones, J. Edwards, M. Dunne, and O. Willi, Phys. Rev. Lett. **74**, 2961 (1995); R. G. Watt, D. C. Wilson, R. E. Chrien, R. V. Hollis, P. L. Gobby, R. J. Mason, R. A. Kopp, R. A. Lerche, D. H. Kalantar, B. MacGowan, M. B. Nelson, T. Phillips, P. W. McKenty, and O. Willi, Phys. Plasmas **4**, 1379 (1997).
[10] J. H. Gardner and S. E. Bodner, Phys. Rev. Lett. **47**, 1137 (1981).
[11] W. M. Manheimer, D. G. Colombant, and J. H. Gardner, Phys. Fluids **25**, 1644 (1982).
[12] M. Dunne, M. Borghesi, A. Iwase, M. W. Jones, R. Taylor, O. Willi, R. Gibson, S. R. Goldman, J. Mack, and R. G. Watt, Phys. Rev. Lett. **75**, 3858 (1995).
[13] T4 Group, Los Alamos National Laboratory Report No. LALP-83-4, 1983.
[14] M. Kado and K. A. Tanaka, J. Plasma Fusion Res. **70**, 877 (1994).
[15] R. Fabbro, Thèse d'Etat, Université de Paris–Sud, 1982; J. Lindl, Phys. Plasmas **2**, 3933 (1995).
[16] Y. B. Zeldovich and Y. P. Raizer, *Physics of Shock Waves and High Temperature Hydrodynamic Phenomena* (Academic, New York, 1967).
[17] J. W. Falconer, W. Nazarov, and C. J. Horsfield, J. Vac. Sci. Technol. A **13**, 1941 (1995).
[18] R. Ramis, R. Schmalz, and J. Meyer-ter-Vehn, Comput. Phys. Commun. **49**, 475 (1988).
[19] M. Busquet, Phys. Fluids B **5**, 4191 (1993).
[20] K. Eidmann and T. Kishimoto, Appl. Phys. Lett. **49**, 377 (1986).
[21] T. Mochizuki, T. Yabe, K. Okada, M. Hamada, N. Ikeda, S. Kiyokawa, and C. Yamanaka, Phys. Rev. A **33**, 525 (1986).
[22] M. Chaker, H. Pépin, V. Bareau, B. Lafontaine, I. Tounhans, R. Fabbro, and B. Faral, J. Appl. Phys. **63**, 892 (1988).
[23] D. Batani, A. Giulietti, L. Palladino, G. Tallents, and E. Turcu, Proc. SPIE **1503**, 479 (1991).
[24] R. Kelly, J. Phys. Chem. Ref. Data Suppl. **16**, No. 1 (1987).
[25] H. Gordon, M. G. Hobby, and N. J. Peacock, J. Phys. B **13**, 1985 (1980).
[26] R. J. Hutcheou, L. Cooke, M. H. Key, C. Lewis, and G. E. Bromage, Phys. Scr. **21**, 89 (1980).
[27] B. L. Henke, E. M. Gullikson, and J. C. Davis, At. Data Nucl. Data Tables **54**, 181 (1993).
[28] R. M. More, Adv. At. Mol. Phys. **21**, 305 (1985).
[29] D. Batani, A. Benuzzi, M. Koenig, B. Faral, M. Temporal, W. Nazarov, T. Hall, and N. Granjouan, Plasma Phys. Controlled Fusion **40**, 1567 (1998).
[30] P. Mora, Phys. Fluids **25**, 1051 (1982).
[31] K. Eidmann, Laser Part. Beams **12**, 223 (1993).
[32] J. S. Cohen and R. H. Clark, Los Alamos National Laboratory Report No. 96-3629, 1996.
[33] T. Hall, A. Benuzzi, D. Batani, D. Beretta, S. Bossi, B. Faral, M. Koenig, J. Krishnan, Th. Löwer, and M. Mahdieh, Phys. Rev. E **55**, R6356 (1997).
[34] A. Benuzzi, M. Koenig, B. Faral, J. Krishnan, F. Pisani, D. Batani, S. Bossi, D. Beretta, T. Hall, S. Ellwi, S. Hüller, J. Honrubia, and N. Grandjouan, Phys. Plasmas **5**, 6 (1998).
[35] T. Afshar-rad, M. Desselberger, M. Dunne, J. Edwards, J. M. Foster, D. Hoarty, M. W. Jones, S. J. Rose, P. A. Rosen, R. Taylor, and O. Willi, Phys. Rev. Lett. **73**, 74 (1994).
[36] J. Massen, G. D. Tsakiris, K. Eidmann, I. B. Foldes, Th. Lower, R. Sigel, S. Witkowski, H. Nishimura, T. Endo, H. Shiraga, M. Takagi, Y. Kato, and S. Nakai, Phys. Rev. E **50**, 5130 (1994).
[37] R. J. Mason, R. A. Kopp, H. X. Vu, D. C. Wilson, S. R. Goldman, R. G. Watt, M. Dunne, and O. Willi, Phys. Plasmas **5**, 211 (1998).
[38] A. L. Velikovich, J. P. Dahlburg, J. H. Gardner, and R. J. Taylor, Phys. Plasmas **5**, 1491 (1998).
[39] V. N. Goncharov, Phys. Rev. Lett. **82**, 2091 (1999).
[40] R. J. Taylor, A. L. Velikovich, J. P. Dahlburg, and J. H. Gardner, Phys. Rev. Lett. **79**, 1861 (1997).